CHALMERS
UNIVERSITY OF TECHNOLOGY

Experimental investigation on prevalent local failure mechanisms in hard rock tunnel linings using distributed optical fibre sensors

Engineering Structures 333 (2025) 120185

Contents lists available at ScienceDirect

Engineering Structures

journal homepage: www.elsevier.com/locate/engstruct

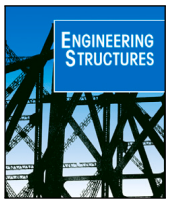

Experimental investigation on prevalent local failure mechanisms in hard rock tunnel linings using distributed optical fibre sensors

August Jansson [a,*], Andreas Sjölander [b], Carlos G. Berrocal [a], Rasmus Rempling [a,c], Ignasi Fernandez [a]

[a] Chalmers University of Technology, Sven Hultins gata 4, Göteborg, 412 58, Sweden
[b] Royal Institute of Technology, Drottning Kristinas väg 4, Stockholm, 100 44, Sweden
[c] NCC, Drakegatan 10, Göteborg, 412 50, Sweden

ARTICLE INFO

Keywords:
Shotcrete
Distributed optical fibre sensors
Structural health monitoring
Strain patterns
Load identification

ABSTRACT

In today's hard rock tunnel construction, the most common support system consists of rock bolts and shotcrete linings. The support system is effective to build, and structural safety has empirically been established. However, the utilization rate of shotcrete linings is usually unknown as no method exists today that determines the type and magnitude of loads acting on the linings. This paper investigates the implementation of distributed optical fiber sensors (DOFS) as a promising solution for monitoring of local loads in shotcrete tunnel linings. This approach enables the identification of local loads, facilitating targeted inspections in areas with deviating measurements and allowing for more informed repair and maintenance decisions. In the study, two typical local load conditions in shotcrete linings were analysed using strain measurements from DOFS installed in experimental specimens designed to replicate sections of tunnel linings. The results revealed that the examined load conditions can be distinguished based on the measured strains. While the lining thickness had a significant effect on the peak load capacity, the roughness of the substrate influenced the strain distribution in linings subjected to bending. It was also shown that DOFS outside the loaded area could detect load-induced strains for shear loaded specimens at low load levels, but not for flexurally loaded specimens.

1. Introduction

Fibre-reinforced sprayed concrete, or shotcrete, is commonly used in combination with rock bolts to support tunnels in hard rock. In a simplified way, the support principle is that rock bolts secure large blocks, while shotcrete supports potentially loose blocks that fit between a group of rock bolts. However, the support system is, in fact, a complex composite structure in which the rock mass is part of both the support system and the external load. The load distribution between the rock-lining system components depends on the quality of the structural connection between the shotcrete, rock bolts and rock mass.

The local failure process in a shotcrete lining typically starts with bond failure between the shotcrete and the rock, which partly reduces the composite action of the support system. As the bond fails, the shotcrete layer is instead supported by the rock bolts, and it can then be considered as a concrete slab [1,2]. Further, the bond strength typically presents a high variability [3] and it is hard to determine, hence a conservative design approach based on the residual flexural strength of the shotcrete is often adopted in design.

For global stability analysis of a tunnel structure, the shotcrete lining can be regarded as a shell, where the in-plane stiffness of the lining is utilized to resist the rock mass deformation that occurs after excavation [4]. The in-plane stress that arises in the lining from the rock mass deformation will contribute to the out-of-plane local failure resistance through membrane action and the magnitude of the in-plane stresses will depend on the stiffness relation between the lining and the rock as well as the tunnel section geometry. Blasted hard rock tunnels are usually built with open sections and irregular geometries, leading to relatively small in-plane stresses compared to oval or circular tunnel sections.

A common approach to calculate the local capacity of the shotcrete lining is assuming that the force from a loose block is transferred to the surrounding rock mass through bond stresses distributed over a narrow band around the perimeter of the loose block [1,5,6]. Based on experimental results, Holmgren [5] and Fernandez-Delgado et al. [6] suggested that the width of the band only has a weak correlation to the shotcrete thickness. Thus, the structural capacity with respect to

* Corresponding author.
E-mail address: august.jansson@chalmers.se (A. Jansson).

https://doi.org/10.1016/j.engstruct.2025.120185
Received 18 November 2024; Received in revised form 12 February 2025; Accepted 17 March 2025
Available online 29 March 2025

the failure load of the bond P_{bond} is not affected by the thickness of the shotcrete. However, based on numerical simulations using the finite element method, contradictory results were presented by Sjölander et al. [7], which showed a strong linear correlation between P_{bond} and the mean shotcrete thickness around the perimeter of the block.

Several authors have studied the influence of surface roughness and treatment in the past, see e.g. [8–12]. For instance, Hahn et al. [10] studied the correlation between surface roughness, mineral composition and bond strength concluding that mineral composition has the most significant influence but that the bond strength is usually higher for a rough surface compared to a smooth surface. Malmgren et al. [11] investigated whether the rock scaling method affected the bond strength and compared mechanical scaling to water-jetting at 22 MPa water pressure. The surface scaled with water-jetting clearly showed a higher bond strength. However, as discussed in Sjölander [13], the failure mode also changed. For mechanical scaling, failure occurred more frequently in the rock mass, while interface failure was dominant for water-jetting. Thus, even though the test indicates higher loads, it does not necessarily show that water-jetting affects the bond strength between shotcrete and rock. However, it does show that removing fractured and low-quality rock increases the structural capacity of a bonded shotcrete lining.

When shotcrete is loaded by a loose block, the stiffness of the rock block will affect the structural response and cracking of the shotcrete lining. However, in reported experiments [5,6], the load was applied by a combination of stiff steel plates, a hydraulic jack and a block of concrete or rock. Thus, the block previously used had a rather high stiffness whereas to the authors' knowledge, no experiments with soft blocks, or, distributed loose rock material have been reported. Bjureland et al. [2] investigated the influence of the block stiffness numerically. The stiffness varied between 0 and 10 GPa and the results indicated that the load-bearing capacity for the shotcrete increased with an increased block stiffness in the range between 0 and 3 GPa. The capacity was thereafter more or less constant.

Despite the widespread use of shotcrete and its design complexity, large scale tests are scarce and characterizations of load conditions, load-induced cracking and bond behaviour between rock and shotcrete are lacking. Furthermore, monitoring of tunnels is an essential activity during construction to ensure both the safety requirements and the function of the structural elements [14]. Among several other parameters, convergence and lining strains are usually monitored with discrete measuring methods such as total station surveying and strain gauges, respectively. In hard rock tunnels, delamination between rock and shotcrete is inspected by knocking at the surface with a hammer and listening for hollow sounds. The precision when using discrete measuring techniques is highly dependent on the number of measurement points and the hammer knocking inspections are highly subjective, as the results depend on the experience and skill of the inspector. By installing Distributed Optical Fiber Sensors (DOFS) in the lining continuous measurements can be obtained along the lining and recent studies have shown their usefulness in measuring strains and consequently convergence of the tunnel [15,16]. However, in the above mentioned studies, DOFS based on the Brillouin scattering technique were used. This technique provides a lower spatial resolution, compared to measurements based on Rayleigh backscattering. For concrete structures, the Rayleigh backscattering technique with a spatial resolution in the sub-millimeter scale, enables the detection and location of cracks as well as the quantification of crack widths with high accuracy [17]. A drawback with Rayleigh backscattering is the maximum range of 100 m compared to the Brilluoin range up to 200 km [18]. By monitoring tunnel lining sections with Rayleigh back-scattering DOFS, in addition to obtaining the tunnel convergence, the analysis of strain patterns could be used to identify the distribution of loads on the lining due to the loss of bond or the presence of rock blocks and loose rock material, both during the construction phase and the service life.

Therefore, the present study aims to investigate the suitability of DOFS as basis for an enhanced inspection and monitoring solution for shotcrete linings. By analysing the strain data from the DOFS sensors, the identification of strain patterns that correspond to specific loading conditions, e.g. block load, distributed loose rock mass and bond loss, should be possible, and thus to determine the structural integrity of the shotcrete and optimize maintenance. Thereby, this paper focuses on the identification of such strain patterns in fibre-reinforced and bolt-anchored shotcrete linings subjected to two well defined load conditions: a block load and distributed loose rock mass. This was done through an extensive experimental campaign in laboratory environment. The study also included a variation of shotcrete cover, loaded area and bond quality. In particular, the focus was on the detailed analysis of the strain profiles in order to assess the distribution and magnitude of strains in the serviceability state, i.e., at the onset of cracking before reaching the maximum load of the lining. The influence of in-plane stress distributions are not considered in this study as it would only change the magnitude of strains and not the strain pattern characteristics.

2. Experimental method

The experimental setup was designed to replicate a shotcrete tunnel lining in hard rock exposed to typical load configurations considered in design, namely (i) loads from a loose rock block and (ii) distributed loose rock material [1]. In order to minimize the uncertainties associated to the use of shotcrete, i.e. uniformity in thickness and distribution of material properties, cast fibre reinforced concrete (FRC) was used. Further, cast concrete was also used to substitute the rock substrate material, allowing for different surface treatments and the detailing of load conditions explained in Section 2.1. Thus, the material choice aimed at decreasing the dispersion in results between the different specimens, allowing for a better understanding of the results. As a result, the variation of thickness and material variability that inherently occurs when spraying concrete is disregarded in these experiments. Sjölander [13] showed numerically that the variation of thickness and material variation have a small impact on the load carrying properties of the shotcrete layer and, in this experimental campaign, no specimen was repeated, making it impossible to statistically determine the effect of the variations. Furthermore, as the experiments aim to isolate strain distributions pertaining to load effects, the introduction of material and geometrical variation would impede such analysis. As the material used for these experiments differed from the materials in a real tunnel, the results regarding load values cannot be directly implemented for design of tunnel structures. The optical fibre cables used in this study, Solifos BRUsens V9, have been used in shotcrete linings before, where the shotcrete was sprayed directly on the cable [16].

To investigate the behaviour of the tunnel lining, a full factorial experimental design was implemented with four factors, including load conditions, loading area, lining thickness and interfacial bond strength between the lining and the substrate rock. The factors were chosen with respect to the largest influence on the maximum load based on preliminary modelling results presented in [19]. Each factor in the full factorial design had two levels, resulting in a total of 16 unique specimens.

Experiments similar to the ones in this study have been conducted previously. In the 1970s', Holmgren [5,20] and Fernandez-Delgado et al. [6] investigated the failure modes and load capacity for a bolt-anchored and fibre-reinforced shotcrete lining in interaction with hard rock subjected to a block load. The experimental setups of the previous experiments are shown in Fig. 1. In both tests, a thin layer of concrete was bonded to two substrate blocks in rock or concrete and tested by pushing one of the substrate blocks vertically, shearing the thin concrete layer. It was concluded that the initial failure occurred in the bond between shotcrete and substrate in both studies, and, as mentioned in Section 1, the lining thickness had an insignificant influence on the

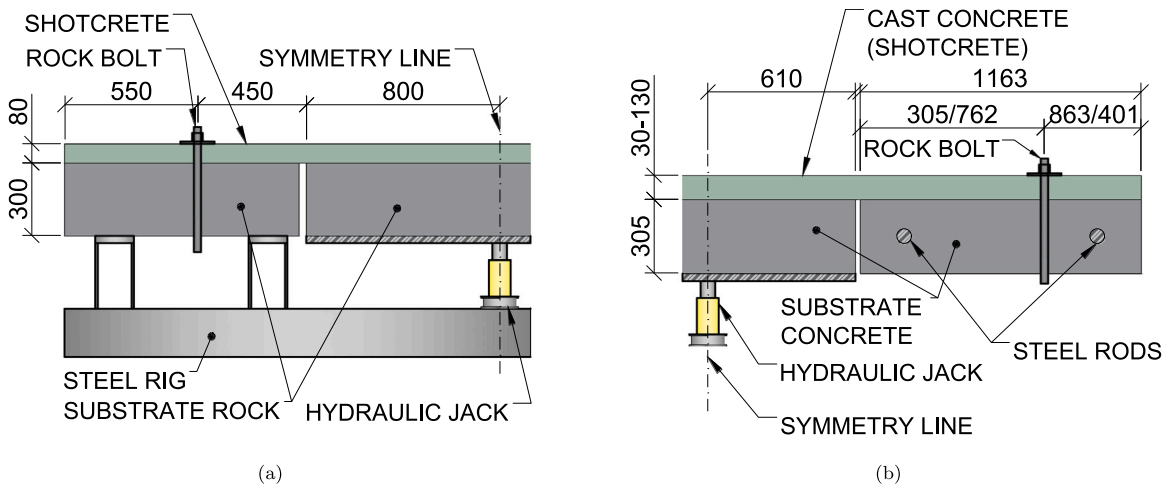

Fig. 1. Geometry and layout of experimental specimens performed by (a) Holmgren [5] and (b) Fernandez-Delgado et al. [6].

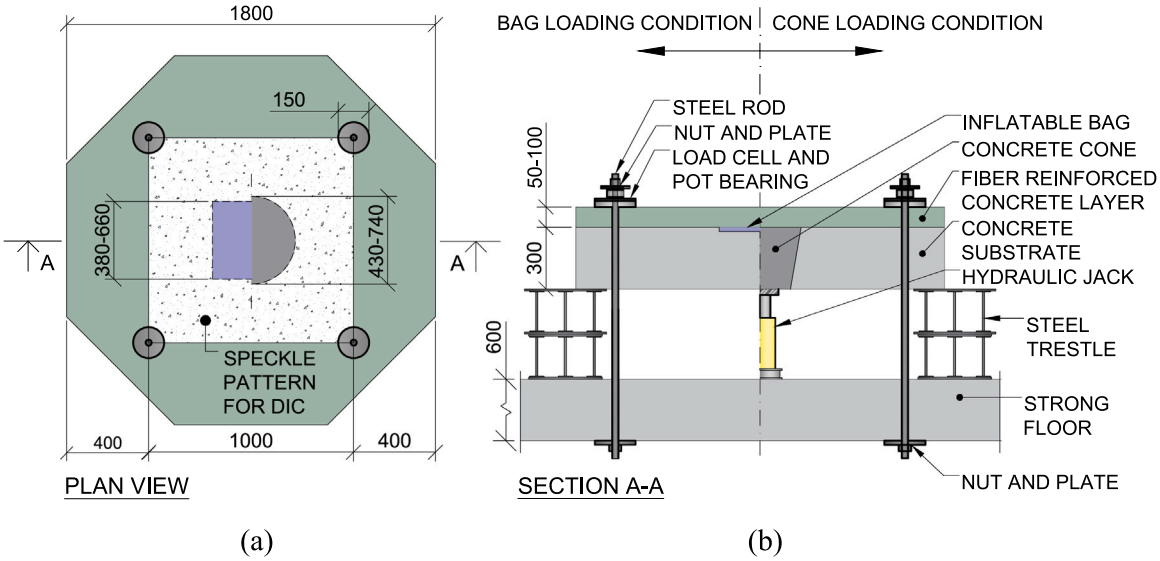

Fig. 2. Geometry and layout of experimental specimens. (a) Plan view of the specimen with right side for cone loading condition and left side for bag loading condition (b) The right half shows the geometry for the cone loading condition and the left half shows the bag loading condition. All measurements in mm.

peak-load. However, a consequence of the setup used in that study is the pronounced 2D behaviour where cracks formed along the perimeter of the block and at the location of the rock bolts. As a result, the crack patterns formed a hinge and any potential redistribution of forces due to 3D effects was not included in the studies.

2.1. Geometry and test setup

The specimens in this study had a symmetrical octagonal shape with a length of 1.8 m across parallel sides and a centrally placed load to include 3D effects present in a shotcrete tunnel lining. The geometry and setup is shown in Fig. 2 and a more complete description of the experiments, as well as the raw experimental data is available in [21]. All specimens consisted of an FRC top layer cast on top of a 0.3 m thick concrete substrate slab. These are denoted FRC top layer and substrate concrete slab in this paper, respectively. Plastic tubes were installed in the corners of a centrally placed square with 1 m sides. The plastic tubes penetrated the whole specimen and steel rods were later installed in the tubes, representing the rock bolts typically anchoring the shotcrete to the rock mass.

To simulate the load from a rock block on a tunnel lining, cones were cast within the substrate concrete slabs and separated from the substrate slab with a steel sheet formwork. During loading, the cones were pushed through the top FRC layer with a hydraulic jack and due to the inclination of the cone side, the transfer of frictional force between the cone and the substrate concrete slab was minimized. The loose rock loading condition was reproduced by installing lifting bags between the two concrete layers. The lifting bags were connected to a hydraulic pump through a tube installed during the casting of the substrate slab. For both loading conditions, cones and lifting bags, two loading area sizes were used. The lifting bags had square shapes with side lengths of either 380 mm or 660 mm and the cones were produced with approximately equal area, resulting in top cone radii of 215 mm and 370 mm, and a bottom cone radii of 160 mm and 310 mm, respectively.

Two thicknesses were used for the top FRC layer, 50 and 100 mm, and two surface treatment methods were applied to the substrate concrete slabs, namely grinding and hydro-demolition. The surface treatment procedures were performed to influence the inter-facial bond strength between the two layers of concrete. As concluded in [22], a ground surface produces a lower bond strength, while a hydro-demolished surface produces a higher strength bond between the two layers of concrete. The hydro-demolition was conducted with a 0.7 mm porcelain nozzle at 220 MPa pressure, positioned 15–20 cm from the

Table 1
Factorial design of experiments with four factors. Ground and Hydro are short for ground and hydro demolished surface treatment factors. The abbreviations CS50G, CS100G etc., each represent an individual experimental specimen.

	Loading condition							
	Cone				Lifting Bag			
	Loading area [mm]							
	Small ∅430		Large ∅740		Small 380 × 380		Large 660 × 660	
	Thickness of FRC top layer [mm]							
	50	100	50	100	50	100	50	100
Ground	CS50G	CS100G	CL50G	CL100G	BS50G	BS100G	BL50G	BL100G
Hydro	CS50H	CS100H	CL50H	CL100H	BS50H	BS100H	BL50H	BL100H

Table 2
Results for drilled cores loaded in tension with hydro demolished (H) or ground (G) substrate surface. Mean value in parenthesis does not include specimens failed in the glued interface.

Specimen	1	2	3	4	5	6	7	8
Treatment	G	G	G	G	H	H	H	H
Tensile bond strength [MPa]	2.12	2.44	1.50	3.10	2.00[a]	2.90[a]	2.56	3.46
Mean value [MPa]	2.29				2.73 (3.00)			

[a] Indicates failure in the glued interface with the machine.

concrete surface. For the ground specimens, an OPTIROC ABS8331 grinding machine was used. An overview of the experimental setup is shown in Fig. 2, while Table 1 presents a summary of key features for the different series and the nomenclature for each specimen.

In addition to the slab experiments, drilled cores were tested in uniaxial tension to characterize the inter-facial bond between the top FRC layer and the substrate concrete slab. The cores were glued to steel plates that were fastened to the testing machine, as in [22]. In total, eight cores were tested and the results from these cores are presented in Table 2. Highlighted in the table are two specimens that failed in the glued interface between the specimen and steel plates. The other two hydro-demolished specimens failed in either the substrate concrete or FRC layer. The cores with ground substrate interfaces failed either in the interface or substrate concrete.

2.2. Test procedure

The tests were carried out by placing the specimen on two steel trestles and fixing it to the strong floor using Dywidag ϕ 25 mm steel rods, protruding through the cast-in plastic tubes, and floor anchor points. Steel plates were placed under the floor slab and on top of the specimen and the rods were tightened using a nut and a hand-powered wrench, i.e. the pretension is assumed to be zero. For the cone-loaded specimens, a hydraulic jack was placed on the floor under the specimen and connected to a hydraulic pump. The jack was displacement-controlled at 0.5 mm/min until the peak-load and changed to 2 mm/min thereafter.

Both jack and bags were coupled to a hydraulic oil pressurizing system with a maximum capacity of 300 bar. To physically reduce the maximum pressure in the lifting bags for safety reasons, a double-cylinder system was introduced resulting in a maximum output pressure of 26.5 bars in the lifting bags shown in Fig. 4a. As a consequence of the pressure redistribution in the cylinder system, the maximum amount of hydraulic oil that could be used to fill the lifting bag was restricted. Consequently, during the testing of the bag-loaded specimens, the larger cylinder had to be refilled. When testing specimens with large lifting bags, the cylinder system was refilled up to three times while the small bags required at least two refills. The loading was volume controlled at a rate of 0.213 l/min.

2.3. Measurement and equipment

In all specimens, the top FRC layer was instrumented with Solifos V9 optical cables. A total of four cables were installed in each specimen, covering two directions in the upper and lower face of the top FRC layer. The cables were fastened and tensioned to the formwork prior to the casting of the top FRC layer, oriented in a serpentine pattern with 200 mm between parallel segments of the cables. In Fig. 3, the arrangement of optical fibre cables is shown for a bag-loaded and a cone-loaded specimen, and each cable is denoted with an index. Each cable was protruding through the formwork side at both ends in which either a connector or a termination was installed. During testing, the cables were connected to an Optical Distributed Sensor Interrogator (ODiSI6108) from Luna inc. that measured the distributed strains in the fibre optic cable. The measurement frequency results from a combination between the number of channels, the cable length per channel and the chosen gauge length. A higher frequency results in less channels, shorter cables and larger gauge lengths and vice versa. For all specimens, a configuration consisting of four channels and a gauge length of 5.2 mm was used, which according to the sensor length deployed resulted in a sampling frequency of 6.25 Hz.

The load from the hydraulic jack pushing the cone was measured using a load cell placed underneath the hydraulic jack. Furthermore, three Linear Variable Differential Transformers (LVDTs), spaced at 120°, were glued to the bottom of the substrate slab, measuring the displacement of the cone relative to the substrate slab as shown in Fig. 4b. The hydraulic jack was displacement controlled using an LVDT attached to the jack and measuring the displacement of the cone. During the loading of the bag-loaded specimens, the pressure in the bags was measured using a pressure cell connected to the tube supplying the bag with hydraulic oil, see Fig. 4a. All LVDTs, the load cell and the pressure cell measured at 8 Hz. The top surface of all specimens was also painted with a high contrast speckle pattern and monitored with the Aramis adjustable 12M stereo camera system, mounted approximately 1.5 m above the specimen during testing, see Fig. 4c. The cameras took photos at a frequency of 0.5 Hz and the pictures were post-processed using digital image correlation (DIC) facilitated by the software GOM Correlate 2018. Due to the stereo camera setup, displacements could be calculated in all directions, XYZ.

3. Results and discussion

In this section, the results from the experiments are presented and the influence of each of the studied factors is discussed. First, loads recorded with load cells and pressure gauges, and displacements measured with LVDTS and DIC are shown, and a comparison between the peak-loads is presented. This is followed by an analysis of pre-peak strains, i.e., strain levels before the peak-load. Finally, the influence of the cable position and, in particular, the possibility to detect loading events not located in the vicinity of the cable are discussed.

3.1. Load-displacement curves

In Fig. 5, load displacement curves for cone loading condition specimens are shown. The initial loading process is plotted on a smaller displacement scale to better show the load development at small displacements, and different scales for the loads have been used to enhance the visualization of the loading process. The displacement shown in Fig. 5 is the mean value from the three LVDTs mounted on the substrate slab. Likewise, Fig. 6 shows the load and displacement curve for the bag-loaded specimens, however, some differences must be noted: the load is calculated as the area of the bag times the pressure in the bag and no LVDT could be installed on the top surface of the specimens which is why the displacement is obtained from the middle point in the DIC deformation field. Note that the scales in Fig. 6 differ both for the displacement and load, as in Fig. 5, to better illustrate the

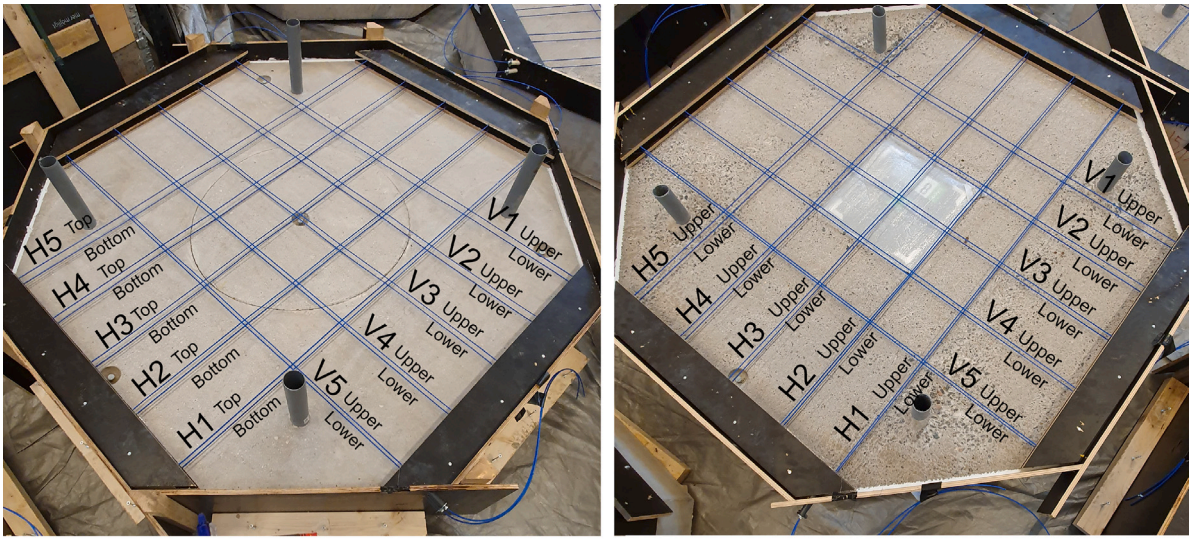

Fig. 3. Optical fibre cable arrangement (blue cables) for (a) bag-loaded specimens and (b) cone-loaded specimens prior to casting of the top FRC layer. (For interpretation of the references to colour in this figure legend, the reader is referred to the web version of this article.)

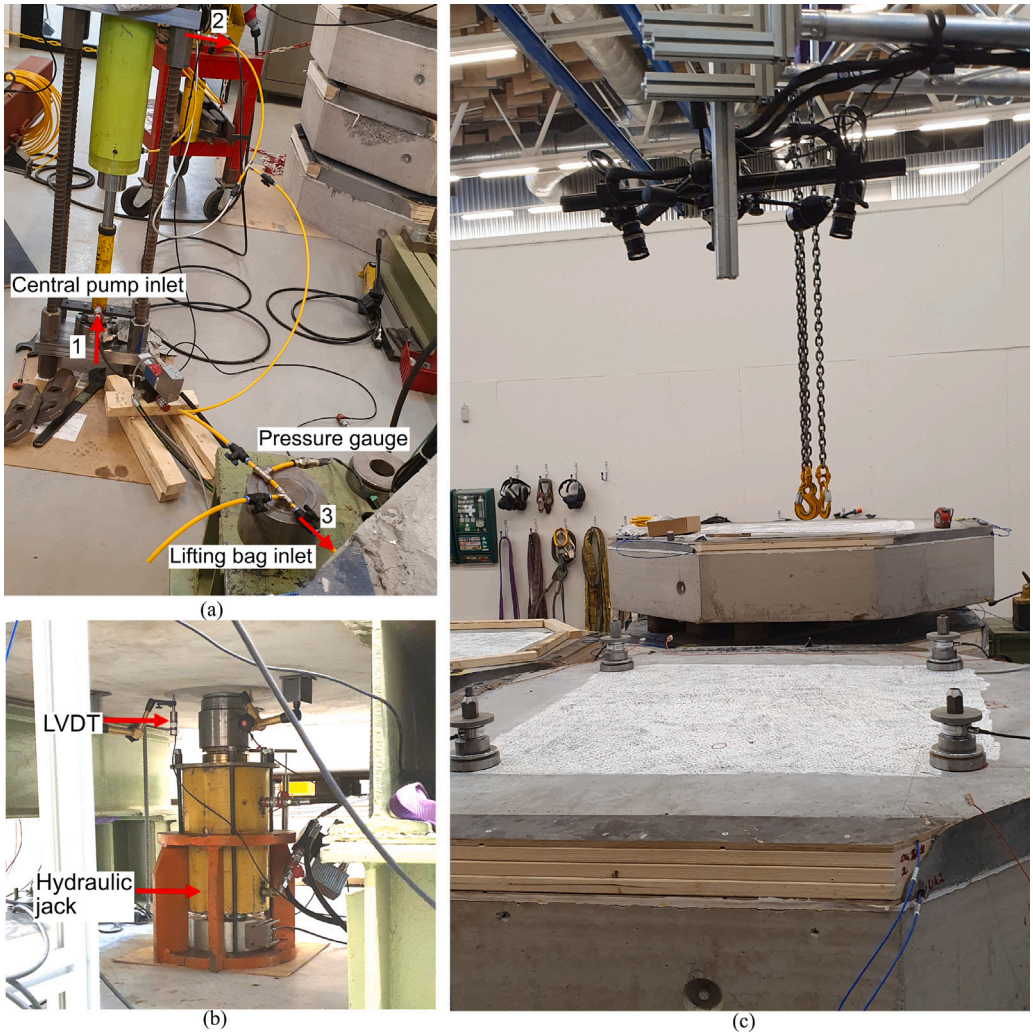

Fig. 4. Measurement techniques and loading devices used during the experimental series. (a) Double cylinder system, pressure gauge and oil inlet for bag-loaded specimens. The direction of oil flow is indicated with arrows and a number sequence from 1 to 3. A specimen is seen in the bottom right corner. (b) Placement of hydraulic jack for cone-loaded specimens and LVDTs mounted underneath the substrate slab. (c) Stereo cameras monitoring the top surface of the specimens and high contrasting pattern painted on the specimen surface.

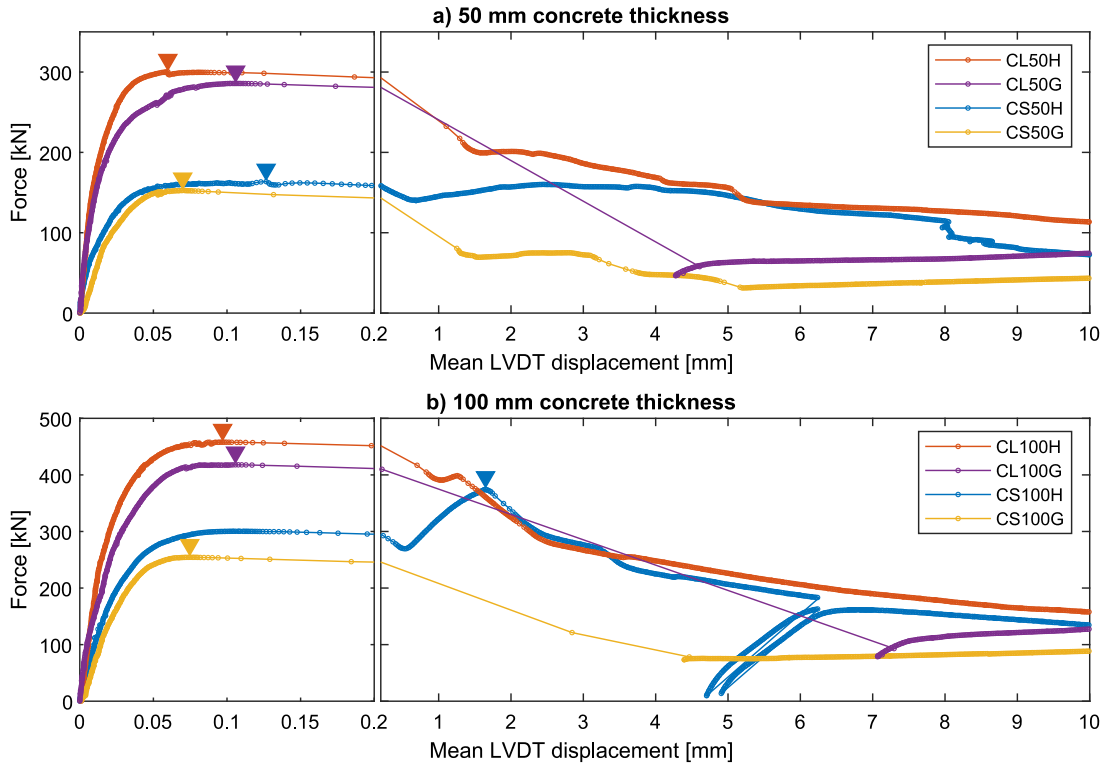

Fig. 5. Load–displacement curves for (a) cone loaded specimens with a 50 mm top FRC layer thickness and (b) cone specimens with a 100 mm top FRC layer thickness. The maximum load reached for each specimen is highlighted with a triangle marker. It should be noted that the scale change at 0.2 mm of displacement in both figures. (For interpretation of the references to colour in this figure legend, the reader is referred to the web version of this article.)

loading process during loading for the different conditions. Further, in specimens BS100G and BS100H the maximum pressure in the bags was reached prior to reaching the load capacity of the specimen. For the cone-loaded specimens, the load increases rapidly before reaching a peak after which the load decreases at different rates. This initial load at small displacements can be compared to the results from [5] where the initial capacity is attributed to the inter-facial bond between the shotcrete and the substrate slab. In Fig. 5, specimens with hydro-demolished surfaces reach slightly higher peak-loads compared to the equivalent ground specimens in all cases. Moreover, after the initial peak load is reached, ground specimens exhibit a distinct drop in load, while the loss of load for the hydro-demolished specimens occurs more progressively and in one case, CS100H, the load even increases.

In contrast, bag-loaded specimens, shown in Fig. 6, exhibit larger displacements before the maximum peak-load is reached. Furthermore, in the hydro-demolished specimens, as loads approach peak-loads, larger deformation occurs, forming a plateau in the curves. The softening following the first peak-load for both loading conditions is, according to [5,6,23], governed by the propagation of the bond failure. Thus, the results indicate that the bond failure of a hydro-demolished surface is more ductile compared to a ground surface and to the authors' knowledge, similar results have not been reported before. Possibly, this could affect the early formation of cracks in the top FRC layer, which is discussed in Section 3.3.

It is clear that the structural behaviour of the top FRC layer differs for the two types of loading condition. Larger displacements occur in the bag-loaded specimens prior to the peak load compared to the cone-loaded specimens. As there is no bond between the top FRC layer and the bags, the pre-peak displacements are probably caused by bending of the top FRC layer in the bag-loaded specimens. In the cone-loaded specimen, as the bond is intact between the cone and the top FRC-layer, composite action between the top FRC-layer and the substrate cone and concrete slab prevents a similar deformation.

3.2. Peak-load

In Fig. 7, the peak-loads for all specimens in Figs. 5 and 6 are summarized. For each sub-figure, the peak-loads of the specimens are compared with regards to one setup factor, indicating the variation by blue and red bars. The blue bars in each sub-figure are sorted from highest to lowest peak-loads and the red bars are mirrored to the blue bars, e.g., the bars closest to the middle (BS50G and CS50G) in Fig. 7a are equal except for the loading condition. The solid and dashed lines indicate the total mean peak-load and the mean peak-load for specimens that reached their maximum load and experienced a load decrease, respectively. For calculation of the mean load for specimens that did not reach their maximum load, both the specimens that did not reach the maximum load, BS100G and BS100H, and the corresponding specimens were excluded. For example, in Fig. 7d both BS100G and BS100H, as well as the corresponding specimens CS100G and CS100H are removed for calculating the mean load of the specimens that reached their maximum load.

From Fig. 7, the most influential factor is the top FRC thickness, with a difference in mean peak-load between a 50 mm and a 100 mm thick slab of 175 kN. In earlier studies [5,6], the shotcrete thickness has been regarded as a low impact factor. In [6], it was concluded that the peak-load applied to the shotcrete layer was almost independent of the shotcrete thickness, whereas in [5], the load was independent of the thickness between 20–80 mm. However, in [7], the shotcrete thickness was identified as a highly influential factor, which is in line with the findings in this paper.

Based on the results with respect to surface treatment, see Fig. 7d, there is a clear tendency that the load-bearing capacity increased for a hydro-demolished surface compared to a ground surface. This is in line with the results from the drilled cores tested in tension and previous research see e.g. [22]. However, the mean ratio of increased peak-load for specimens with hydro-demolished substrate surfaces compared to ground substrate surfaces is larger for bag-loaded specimens than for

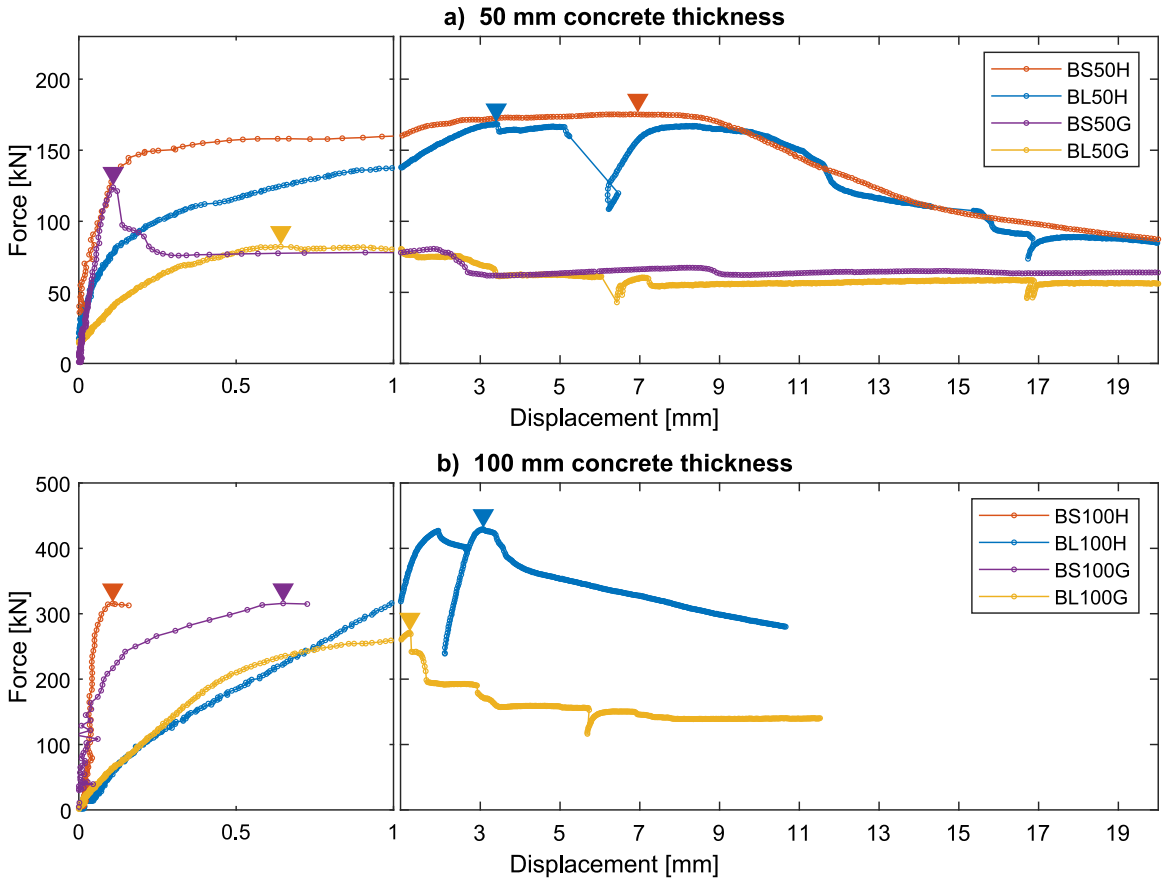

Fig. 6. Load–displacement curves for (a) bag loaded specimens with 50 mm top FRC layer thickness and (b) bag loaded specimens with 100 mm top FRC layer thickness. The maximum load in each specimen is highlighted with a triangle marker. It should be noted that the scale change at 1 mm of displacement in both figures. (For interpretation of the references to colour in this figure legend, the reader is referred to the web version of this article.)

cone-loaded specimens, 1.68 compared to 1.07, respectively, excluding the specimens that did not reach their maximum load capacity. The difference between these ratios could indicate that the bond behaviour is different for bag-loaded and cone-loaded specimens and that bond stresses are distributed differently. This is further discussed in Section 3.3. It is worth noting that the tested bond strength is high compared to results from in-situ testing of bond strength between shotcrete and rock. As an example, Bjureland et al. [3] reported a mean bond strength of 0.81 MPa between shotcrete and rock based on more than 350 samples.

For the load condition and loading area, no clear trends are identified from Fig. 7a-b as the peak-load for a bag-loaded specimen could be lower (compare BL50G and CL50G) and higher (compare BS100G and CS100G) compared to a cone-loaded specimen. To study this further, the data was divided into two sets to identify the interaction on loading area with respect to bag and cone loading as shown in Fig. 8. This figure shows that the load-bearing capacity is greater with a larger loading area for cones, and for bags, the peak-load remain unaffected or even decrease for a larger loading area. A possible explanation for this is that the load-transfer area is affected either by the stiffness of the loading condition or by the lack of bond between the bag and the top FRC layer. As the top FRC layer is unbonded for the bag loading condition, moment forces arise in the top layer, and due to larger spans between bonded areas in specimens with larger bags, larger moments act in the top layer. This is discussed further in Section 3.3.

3.3. Analysis of pre-peak strains

In order to identify loads and potential failure modes prior to failure, the evolution of strain patterns prior to reaching the peak-load are presented and analysed in this section for the two investigated load conditions. Furthermore, differences in strain patterns between the two surface treatments are discussed, and appropriate structural models are suggested to explain the observed behaviour. In Fig. 9a–d, results from the centrally placed optical fibres in both the upper edge and lower edge of the top FRC layer, H3 Upper and H3 Lower from Fig. 3, are presented for two specimens, namely BL100H and CL100H. The strains are presented along the length of the sensors for load-levels ranging from 0% to 90% of the peak-load. Moreover, the curvature in one direction of the same specimens is shown in Fig. 9e–f which is calculated as:

$$\chi = \frac{\varepsilon_{top} - \varepsilon_{bot}}{z} \tag{1}$$

where ε_{top} and ε_{bot} is the top and bottom strains in the cables respectively and z is the distance between the top and bottom optical fibres. The curvatures in this study serve as a means to combine the top and bottom strains for comparisons between specimens and analysis of the top FRC layer behaviour through beam theory. For a more detailed analysis of load effects and deflections, the top FRC layer should be considered as a slab or shell structure. In Fig. 9, a distinct difference in strain patterns can be observed in the top FRC layer between the cone and bag-load conditions. The strain patterns in Fig. 9(a, c) indicate that the FRC top layer is subjected to bending when loaded by a lifting bag with no bond to the FRC top layer. Fig. 9a shows that tensile strains localize centrally over the bag in the top part of the FRC top layer and Fig. 9c shows that tensile strains localize in the lower face of the top FRC layer at the vicinity of the bag boundary. These strain localizations indicates the formation of large single cracks which is likely caused by the lack of bond between the top FRC layer and the bag in combination with the strain-softening behaviour of the FRC

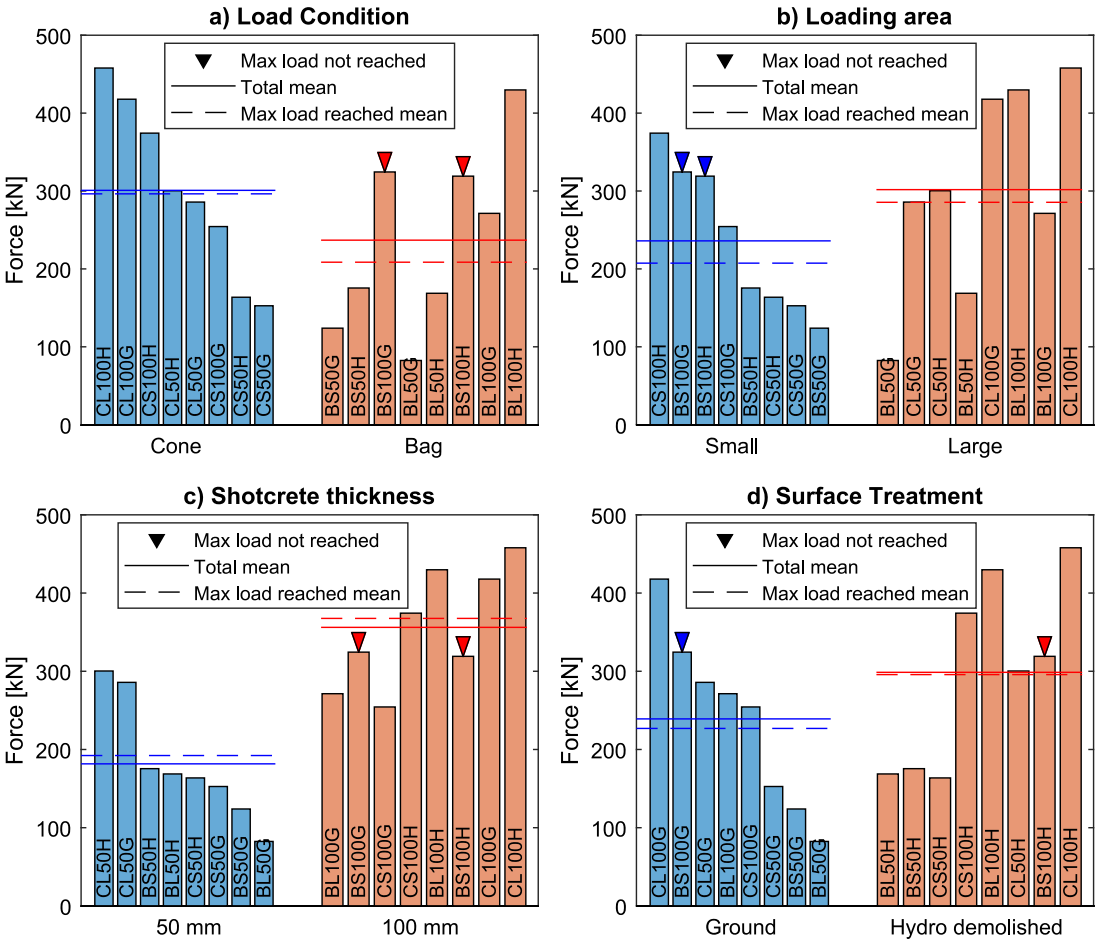

Fig. 7. Peak-loads for each specimen, sorted for the "high and low" values for each factor. (For interpretation of the references to colour in this figure legend, the reader is referred to the web version of this article.)

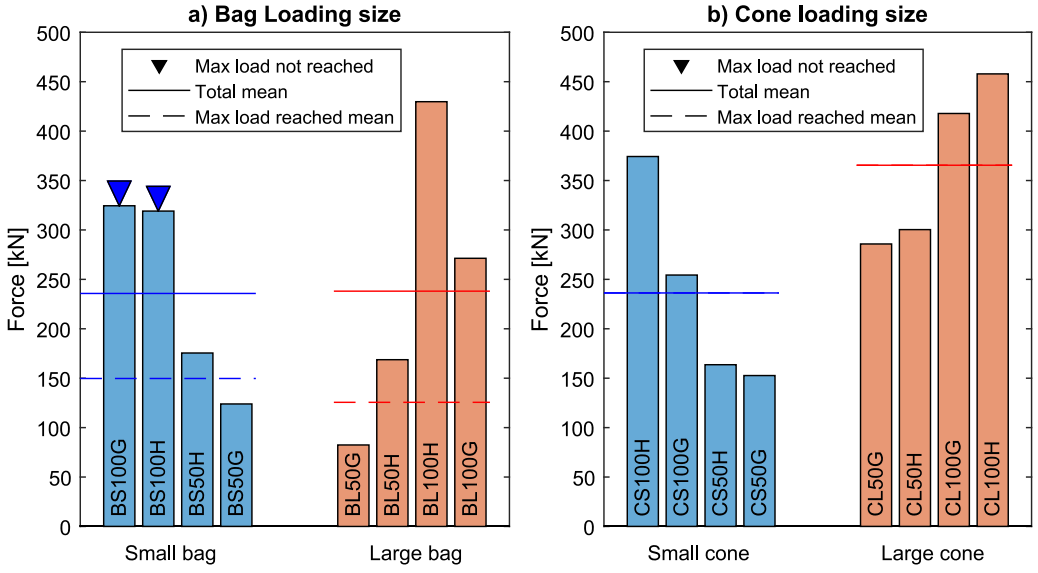

Fig. 8. Loading conditions combined with loading area. Bag-loading condition (a) and cone-loading condition (b).

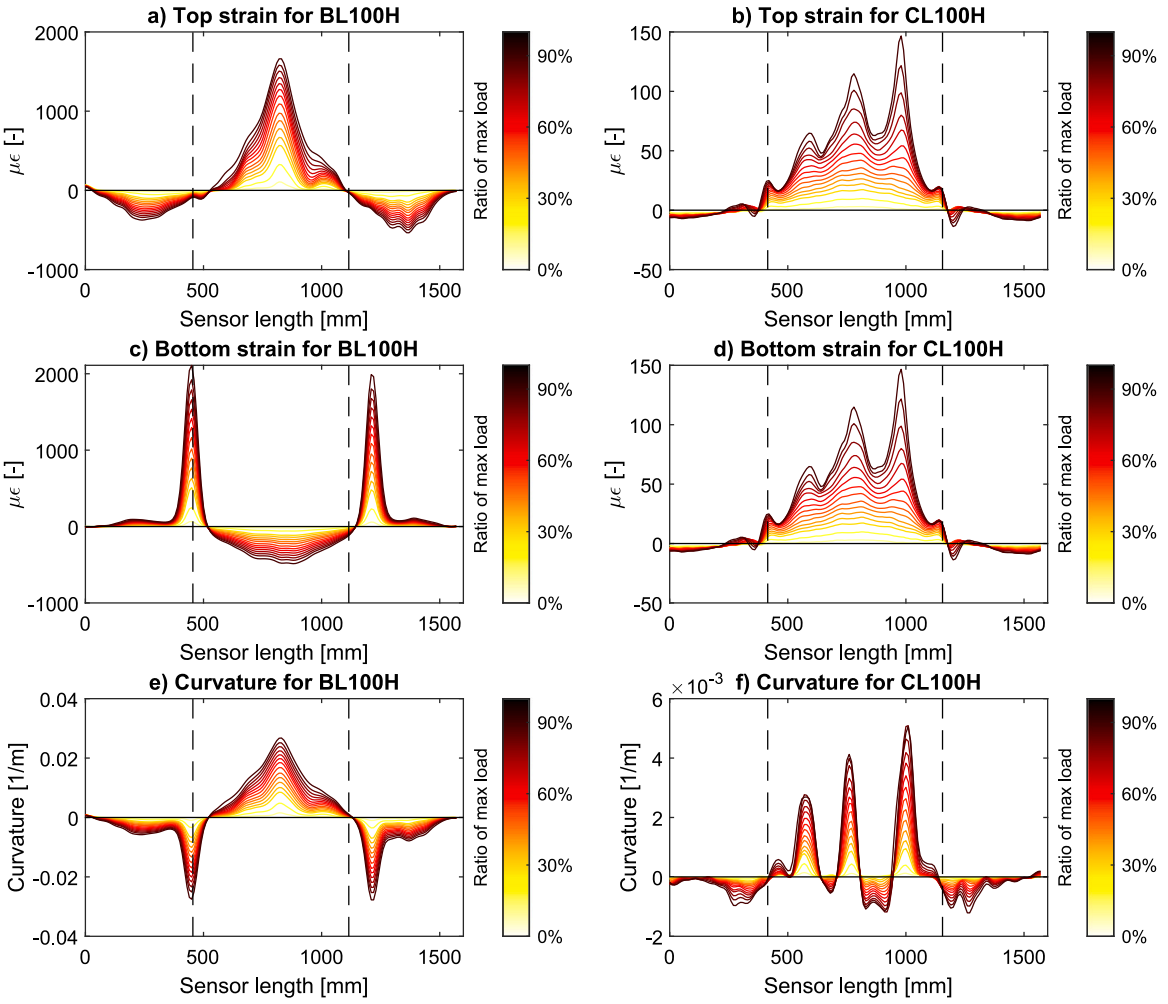

Fig. 9. Pre-peak strain and curvature evolution for centrally placed DOFS for two specimens, bag-loaded BL100H (a), (c) and (d), and cone-loaded CL100H (b), (d) and (f), with hydro-demolished substrate surfaces. The dashed vertical lines indicate the boundaries of the cone and bag.

layer which hinders the possibility of any force redistribution, thereby leading to the formation of large cracks. The behaviour outside of the bag is different; the effect of a strong bond between the top FRC layer and concrete substrate dominates the response. In the close vicinity of the bag, shear and moment forces are transferred, changing into a bending composite action between top FRC layer and substrate concrete further away from the loading area. This bending action outside the bag boundary can be seen in Fig. 9e and a conceptual model of the described mechanical behaviour is presented in Fig. 10(a).

Conversely, while loaded by a cone bonded to the top FRC layer, the strain profiles in Fig. 9(b, d) indicates that tension arises in the top FRC layer as both the upper and lower cables show positive strains. Further, it must be noted that the strains localize in several positions over the cone, which indicates the possible formation of several cracks. This tension can be explained using the strut and tie approach which is applied and shown in Fig. 10(b). As the vertical concentrated load from the hydraulic jack changes direction from a point load to a distributed load in the FRC top layer at the cone boundary, a horizontal tensile tie is formed to equilibrate, resulting in tensile strains in the top FRC layer. The difference in tensile magnitudes between upper and lower DOFS can be explained by the restraint between the cone and top FRC layer. As the top FRC layer is cast on the substrate slab, and cone, horizontal shrinkage restraint is introduced at the interface between the concrete layers which decreases along the thickness of the FRC layer. The degree of restraint is therefore larger at the lower optical fibre cable layer, hence, a smaller magnitude of tensile strains is recorded in the lower DOFS and compressive strains are measured in the top DOFS. It is important to note that the zero strain state of the results presented is referred to the strain state at the start of loading. Consequently, strain changes due to shrinkage or temperature variations between the casting and testing of the specimens are not included in the displayed strain profiles.

From the models presented in Fig. 10, it can be seen that the load is transferred via the top FRC layer to the surrounding FRC layer and substrate slab either as moment and shear forces for the bag-loaded specimens or mainly as shear forces for the cone-loaded specimens. Outside the cone and bag boundary, the top FRC layer and substrate concrete slab will act as a composite element, carrying the load to the rock bolts. However, to enable the composite action between the concrete layers, the bond strength between the layers must be sufficient. As discussed in Section 3.2, the difference in stiffness between the loading conditions can be attributed to the lack of bond between the bag and top FRC layer, seen in Figs. 5 and 6. Since no restraint exists between the bag and top FRC layer, strains localize in cracks over the middle and at the boundary of the bag, allowing for a reduction of stiffness and larger bending deformations. In contrast, as the load is transferred through shear forces in cone-loaded specimens, as soon as cracks appear, failure is reached, hence, a high initial stiffness is achieved and no strain localization occur at the cone boundary prior to reaching the max load.

For the monitoring of a real shotcrete lining using DOFS, discerning between strains stemming from rock loads and other effects such as

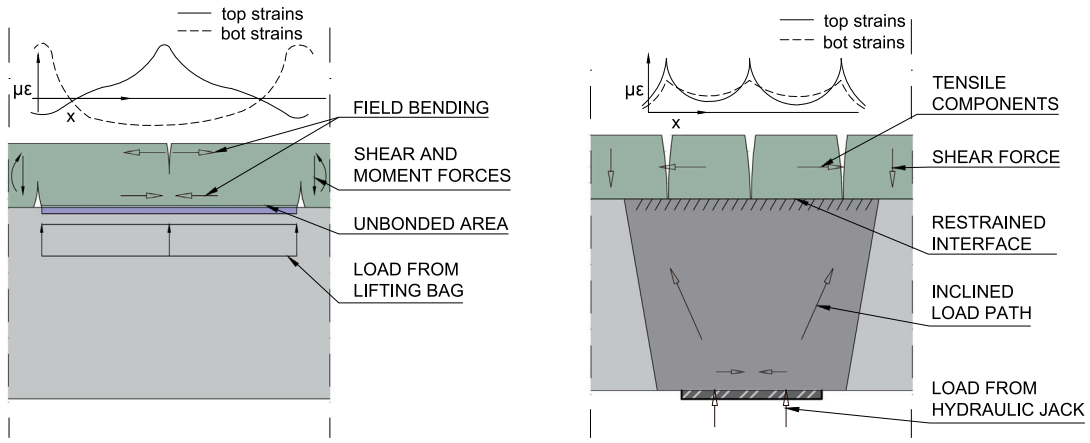

(a) Schematic representation of cracks over the bag, explaining the curvature variation.

(b) Schematic representation of cracks over the cone, explaining the curvature variation. Model for transference of shear forces from top layer FRC to substrate slab.

Fig. 10. Schematic models for load conditions in bag and cone-loaded specimens.

shrinkage and temperature is key in determining the structural integrity of the lining. Strain profiles may be used to identify the boundaries of the loading area and the type of loading, i.e. block or loose rock mass. As the magnitude and sign of strain heavily depends on the cable's distance to the top and bottom surfaces of the concrete layer, by using two parallel cables, with a known separation, determining the curvature will yield more trustworthy data for determining load conditions. Nonetheless, the differentiation between load induced tensile strains, and shrinkage and temperature induced tensile strains requires further investigation.

As discussed in Section 3.1, the substrate surface treatment influence the maximum capacity of the specimens. To further understand how the surface treatment influence the capacity of the top FRC layer, the curvature differences between ground and hydro-demolished specimens will be compared and studied below. In Figs. 11 and 12, more in depth comparisons for analysing the curvature profiles for specimens with identical properties, except for surface treatment methods, are plotted for all failed specimens. As in Fig. 9, the curvatures are plotted up to 90% of the peak-load for each specimen and the peak-load for each specimen is given in the legends. For the bag-loaded specimens, Fig. 11, the curvatures systematically reach higher values in specimens treated with hydro-demolition than for the ground specimens. A similar behaviour cannot be identified in the cone-loaded specimens, Fig. 12, where almost equal strain magnitudes between the two surface treatments can be observed both within and outside of the cone boundary. Furthermore, outside the bag boundaries, the negative curvature in the hydro-demolished bag-loaded specimens spreads further away from the boundaries, compared to the ground specimens.

According to the mechanical model described in Fig. 10(b), the load is expected to be transferred to the surrounding concrete mainly through shear forces in the top FRC layer whereas the bond stresses between the FRC and the substrate concrete are expected to be governed by tensile normal stresses (adhesion), outside the loading area boundaries, see Fig. 13(b). As long as the bond remains within the maximum capacity, the top FRC layer and substrate concrete can be considered working as a composite structure, the shear bond stresses will grow as the moment in the composite structure increases. In Fig. 13(a), shear and normal stresses are schematically shown for bag-loaded specimens in the region outside the loading area boundary. As a moment is introduced in the bag-loaded specimens at the bag boundary, shear bond stresses arise at the boundary of the bag, and compared to the cone-loaded specimen, the bonded interface is subjected to both normal and shear bond stresses. This difference in stress distribution can be used to explain the peak-load variations between the surface treatments. For both surface treatments, similar tensile bond strengths are reached, but the total shear capacities differ most likely due to the roughness of the surfaces, and shear stresses are also carried through friction and mechanical interlocking. In the bag-loaded specimens, assuming that a hydro-demolished surface yields a higher shear stress capacity of the bond due to more friction and enhanced mechanical interlocking, the total bond capacity is expected to be higher, resulting in distributed strains further away the bag boundary, and consequentially a higher peak-load can be reached compared to ground specimens.

3.4. Cable position

In order to study the capacity of DOFS to detect the different loading types at different positions within the specimen area, in Fig. 14, strain values acquired from the upper layer DOFS in one direction are plotted on principal strains calculated using DIC for three load levels. The strains acquired from the DIC are plotted in gray scale to better distinguish from the colourized DOFS strains. At the lowest load level, 30% of the peak-load, a crack can be identified from the DIC measurements in the cone, Fig. 14b, but not for the bag specimen, Fig. 14a. However, the crack detected in the cone specimen at this load level did not intersect the DOFS cables, which display tensile strains localized along the length of the cone and for all cables across the specimen. The bag-loaded specimen, on the other hand, only measured strains in the cable over the bag. The maximum strain in each sensor is shown in a bar plot next to the corresponding sensor.

At the first load level, 30% of the peak-load, high strains can be discerned in the middle DOFS in both specimens. In the cone-loaded specimens, similar strain patterns are also visible in the cables at the cone boundaries and outer fibre cables. Conversely, low or no strains arise in the cables at the bag boundaries and outer DOFS for the bag specimens. The strain patterns in the cone-loaded specimen indicate tension in the top layer, which is in line with the model shown in Fig. 10(b) as radial stresses arise when accounting for the 3D behaviour. For the load level of 60% of the peak load, strains in the middle DOFS increase further in the bag-loaded specimen, Fig. 14c, as cracks localize over the bag. In the cone-loaded specimen, Fig. 14d both middle and intermediate strains increase as tensile strains are distributed over the cone. In the final load level, 90%, similar behaviour as for the 60% load level is exhibited for the cone specimen, Fig. 14e, and in the bag-loaded specimen, cracks localize both in the middle and at the intermediate sensors, Fig. 14f.

The strain level in the outermost cable for the cone-loaded specimen goes from approximately 50% of the maximum strain for the 30% load

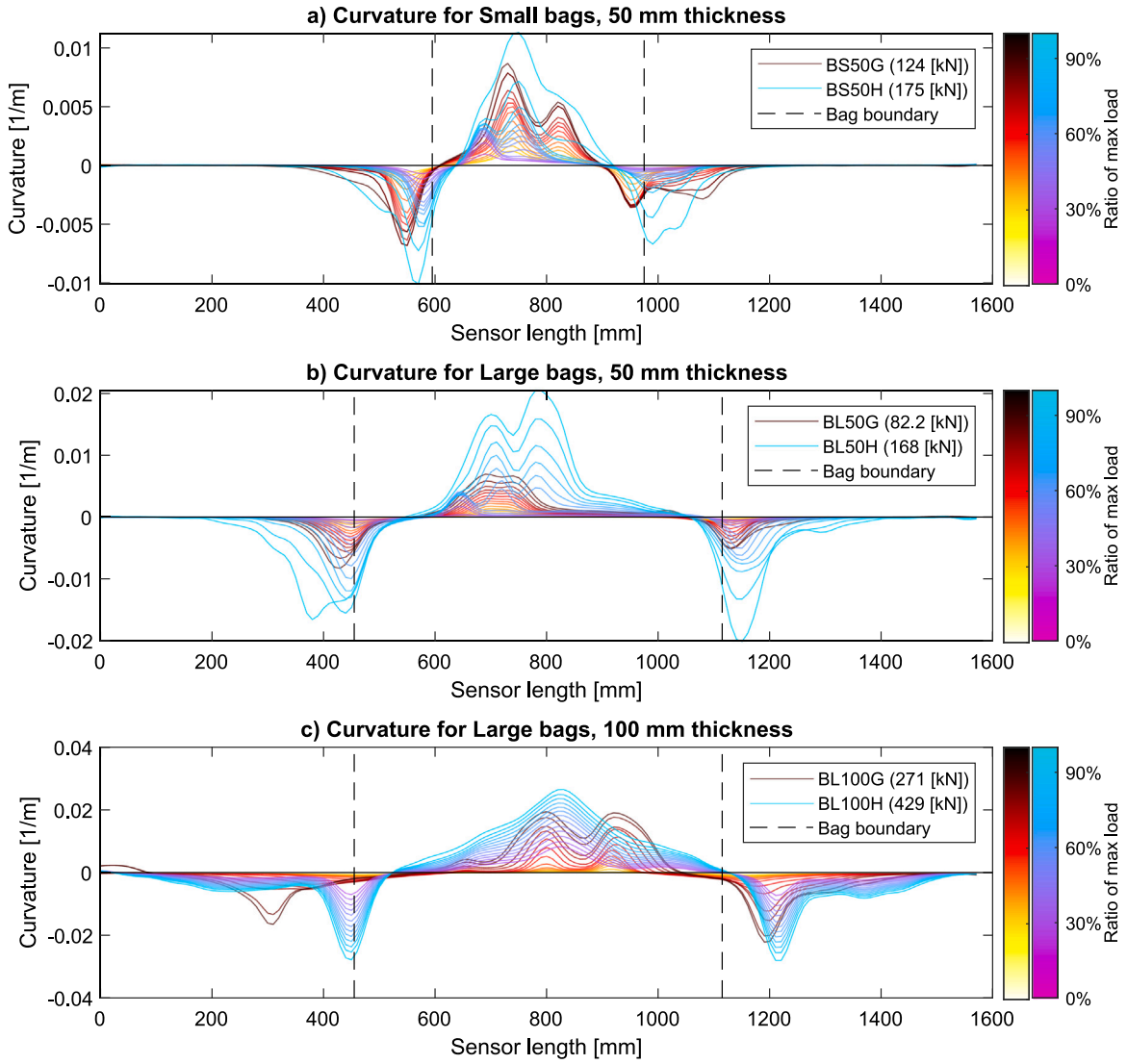

Fig. 11. Curvature evolution for bag loaded specimens. Specimens with ground surface treatments are plotted in the yellow–red colour scale and specimens with a hydro-demolished surface treatment are plotted with the magenta-blue colour scale. (For interpretation of the references to colour in this figure legend, the reader is referred to the web version of this article.)

level, to about only 10% of the maximum strain at a 90% load-level. This can be attributed to the pronounced strain localization caused by the formation of a large crack. Conversely, the strain levels in the cables located at the cone boundary increase significantly at 60% and 90% of the peak load, which can be explained by the progressive formation of cracks perpendicular to the direction of the sensor.

For the bag-loaded specimens, the measured strains indicate the existence of tensile and compressive strains in the top cable at a load level of 30% of the maximum load. When the load level increases, several cracks form but the strain localization is even more pronounced for this case compared to the cone specimen and the relative difference in strain levels between the centric and the sensors at the bag boundaries and outer sensors is much higher compared to the cone-loaded specimen. This may be explained by the lack of bond between the bag and the top FRC layer which results in more localized bending of the FRC layer compared to the cone-loaded specimen. Nevertheless, both cases highlights the difficulty in detecting cracks far away from the sensors. Thus, if DOFS are used in tunnel applications to identify damage caused by loose blocks, the sensors would need to be placed over or very close to the loaded area. To identify damage caused by loose rock mass, the optical cables must be, however, placed over the loaded area in order to effectively detect the load.

4. Conclusions

In this study, the structural behaviour of fibre reinforced shotcrete linings has been experimentally investigated by simulating two typical loading conditions, loose rock blocks and distributed loose rock mass. The block load was simulated as a concrete cone, pushed through the FRC layer, and the loose rock mass load was simulated by inflating a lifting bag cast in between the FRC layer and substrate layer. A factorial design including load condition, loading area, thickness of the FRC layer and surface treatment of the substrate layer was implemented. From this study, the following conclusions can be drawn:

- Based on the test results it was observed that the load capacity of the lining is primarily influenced by the thickness of the FRC layer, where thicker linings yield higher load capacities. When the substrate surface was hydro-demolished, an increased load capacity was also observed compared to ground surfaces, although the effect was only marginal in cone-loaded specimens. Conversely, a larger loading area resulted in higher load capacity for cone-loaded specimens while it had no significant effect on bag-loaded specimens.

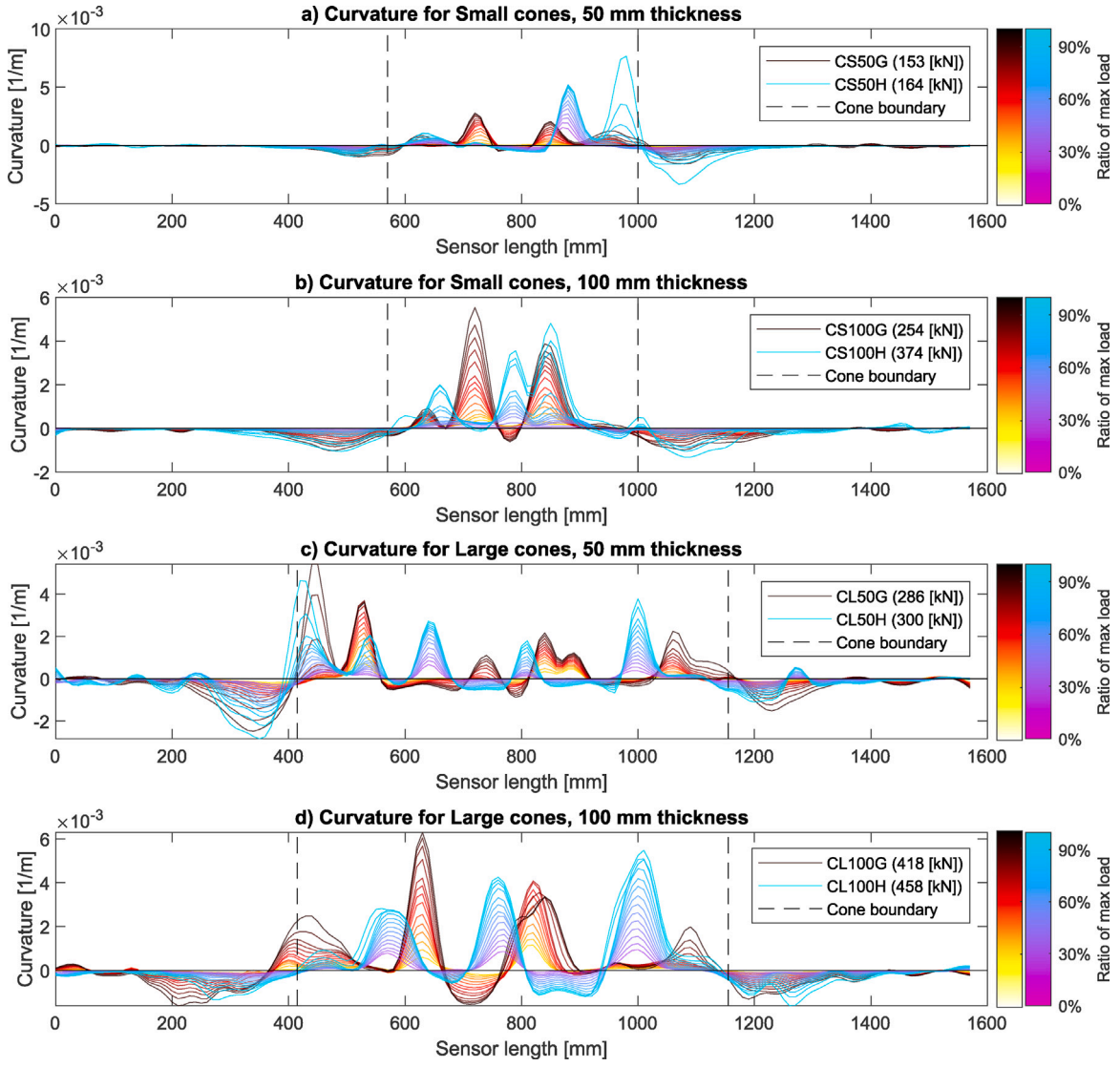

Fig. 12. Curvature evolution for cone loaded specimens. Specimens with ground surface treatments are plotted in the yellow-red colour scale and specimens with a hydro-demolished surface treatment are plotted with the magenta-blue colour scale. (For interpretation of the references to colour in this figure legend, the reader is referred to the web version of this article.)

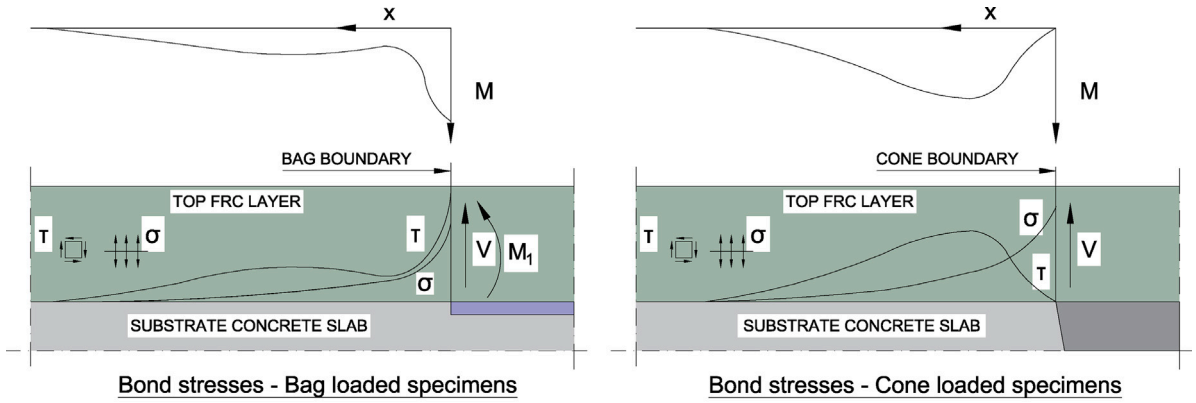

Fig. 13. Schematic representation of shear and tensile bond stresses at the cone and bag boundary.

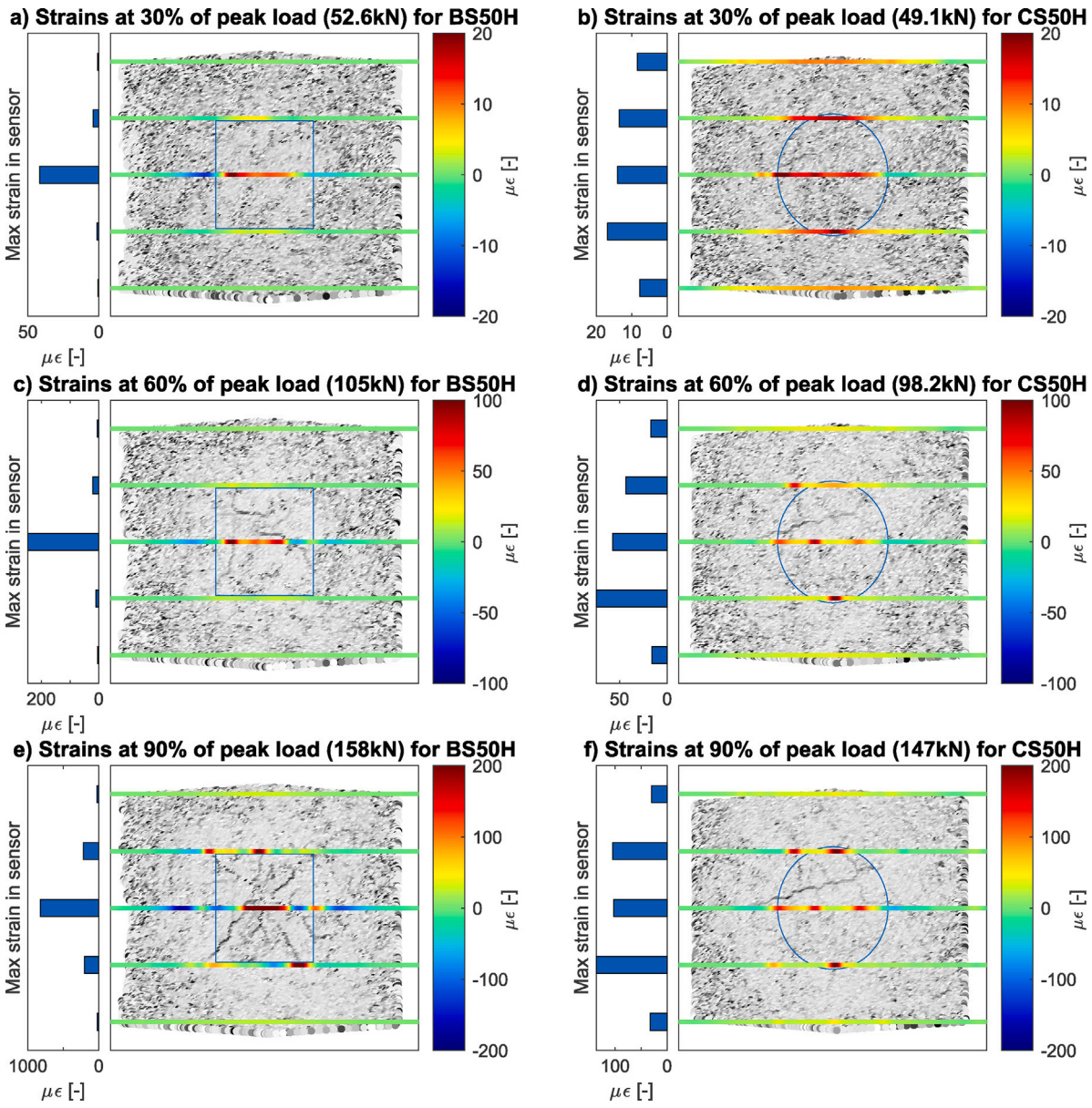

Fig. 14. Strains from DOFS plotted on top of strains obtained from DIC for CS50H and BS50H. The strain measurements from the DIC are plotted in gray scale to better indicate the location of cracks. (For interpretation of the references to colour in this figure legend, the reader is referred to the web version of this article.)

- The monitoring of distributed strains with DOFS revealed clear differences in the deformation behaviour between the two loading conditions investigated. The most remarkable difference was a sharp localization of strains close to the substrate along the boundary of the inflatable bags, which was not observed at the boundary of the cones. Furthermore, while cracks formed over both the cone and bag-loaded specimens, the magnitude of strains measured in the latter were substantially larger.
- Two models were introduced to explain the structural behaviour of the top FRC layer. A strut and tie approach was used for the cone-loaded specimens and fixed translational and rotational boundary conditions were used for the bag-loaded specimens. The models validate the strain profiles measured in the DOFS and highlight the difference between bond stresses arising in bag-loaded and cone-loaded specimens. In bag loaded specimens, both normal and shear bond stresses occur, while mainly normal stresses between the top FRC layer and substrate concrete occur in the cone-loaded specimens.
- The optical fibre cables placed over the loaded area measured strain patterns associated with the studied load-condition for all load levels, 30%, 60% and 90% of the peak load. In the cone-loaded specimens, strains were also present in cables on the cone boundary for the lower load level, 30% of peak-load, while cables on the bag boundaries in the bag-loaded specimens started recording strains at least at 60% of the peak-load. Consequentially, in order to detect loads from loose rock material for service state load levels, the optical cables must be placed over, or very close to, the loaded area, while loads from loose rock blocks can be detected at low load levels when the cables are placed at least 200 mm from the load.

CRediT authorship contribution statement

August Jansson: Writing – review & editing, Writing – original draft, Visualization, Methodology, Investigation, Formal analysis, Data curation. **Andreas Sjölander:** Writing – review & editing, Writing

– original draft, Supervision, Investigation, Formal analysis, Conceptualization. **Carlos G. Berrocal:** Writing – review & editing, Supervision, Methodology, Investigation, Formal analysis, Conceptualization. **Rasmus Rempling:** Writing – review & editing, Supervision, Project administration, Methodology, Investigation, Funding acquisition, Formal analysis, Conceptualization. **Ignasi Fernandez:** Writing – review & editing, Supervision, Project administration, Methodology, Investigation, Funding acquisition, Formal analysis, Conceptualization.

Funding information

This work was supported by the Swedish Transport Administration (Trafikverket) under the grant TRV/BBT 2020-006.

Declaration of competing interest

The authors declare that they have no known competing financial interests or personal relationships that could have appeared to influence the work reported in this paper.

Data availability

The data is available in a separately published data paper, see reference 21.

References

[1] Barrett S, McCreath D. Shortcrete support design in blocky ground: Towards a deterministic approach. Tunn Undergr Space Technol 1995;10(1):79–89. http://dx.doi.org/10.1016/0886-7798(94)00067-U.

[2] Bjureland W, Johansson F, Spross J, Larsson S. Influence of spatially varying thickness on load-bearing capacity of shotcrete. Tunn Undergr Space Technol 2020;98:103336. http://dx.doi.org/10.1016/j.tust.2020.103336.

[3] Bjureland W, Johansson F, Sjölander A, Spross J, Larsson S. Probability distributions of shotcrete parameters for reliability-based analyses of rock tunnel support. Tunn Undergr Space Technol 2019;87:15–26. http://dx.doi.org/10.1016/j.tust.2019.02.002.

[4] Lackner R, Mang HA. Cracking in shotcrete tunnel shells. Eng Fract Mech 2003;70:1047–68. http://dx.doi.org/10.1016/S0013-7944(02)00165-0.

[5] Holmgren J. Punch-loaded shotcrete linings on hard rock. Tech. rep., Stockholm, Sweden: Rock Engineering Research Foundation; 1979.

[6] Fernandez-Delgado G, Mahar J, Cording E. Shotcrete: Structural testing of thin liners. Tech. rep., Washington, USA: University of Illinois; 1975.

[7] Sjölander A, Ansell A, Malm R. Variations in rock support capacity due to local variations in bond strength and shotcrete thickness. Eng Fail Anal 2021;128:105612. http://dx.doi.org/10.1016/j.engfailanal.2021.105612.

[8] Bernard E. Early age load resistance of fibre reinforced shotcrete linings. Tunn Undergr Space Technol 2008;23(4):451–60. http://dx.doi.org/10.1016/j.tust.2007.08.002.

[9] Bryne L, Ansell A, Holmgren J. Laboratory testing of early age bond strength of shotcrete on hard rock. Tunn Undergr Space Technol 2014;41:113–9. http://dx.doi.org/10.1016/j.tust.2013.12.002.

[10] Hahn T. Adhesion of shotcrete to various types of rock surfaces. Report 55, Stockholm, Sweden: Rock Engineering Research Foundation; 1983.

[11] Malmgren L, Nordlund E, Rolund S. Adhesion strength and shrinkage of shotcrete. Tunn Undergr Space Technol 2005;20(1):33–48. http://dx.doi.org/10.1016/j.tust.2004.05.002.

[12] Moradian Z, Ballivy G, Rivard P. Application of acoustic emission for monitoring shear behavior of bonded concrete rock joints under direct shear test. Can J Civ Eng 2012;39(8):887–96. http://dx.doi.org/10.1139/l2012-073.

[13] Sjölander A. Analyses of shotcrete stress states due to varying lining thickness and irregular rock surfaces. Licentiate Thesis. KTH Royal Institute of Technology. Stockholm, Sweden: KTH Royal Institute of Technology; 2017.

[14] Hoult NA, Soga K. Sensing solutions for assessing and monitoring tunnels. vol. 1, Woodhead Publishing Limited; 2014, p. 309–46, URL http://dx.doi.org/10.1533/9781782422433.2.309,

[15] Monsberger CM, Lienhart W. Distributed fiber optic shape sensing along shotcrete tunnel linings: Methodology, field applications, and monitoring results. J Civ Struct Heal Monit 2021;11:337–50, URL https://doi.org/10.1007/s13349-020-00455-8.

[16] Battista ND, Elshafie M, Soga K, Williamson M, Hazelden G, Hsu YS. Strain monitoring using embedded distributed fibre optic sensors in a sprayed concrete tunnel lining during the excavation of cross-passages. In: SHMII 2015 - 7th international conference on structural health monitoring of intelligent infrastructure. 2015.

[17] Berrocal CG, Fernandez I, Rempling R. Crack monitoring in reinforced concrete beams by distributed optical fiber sensors. Struct Infrastruct Eng 2021;17:124–39, URL https://doi.org/10.1080/15732479.2020.1731558.

[18] Barrias A, Casas JR, Villalba S. A review of distributed optical fiber sensors for civil engineering applications. Sensors (Switzerland) 2016;16. http://dx.doi.org/10.3390/s16050748.

[19] Jansson A, Berrocal CG, Fernandez I, Rempling R. Experimental design for shotcrete tunnel lining with distributed optical fibre monitoring. Stockholm: Swedish Concrete Assosiation; 2022,

[20] Holmgren J. Bolt-anchored, steel-fibre-reinforced shotcrete linings. Tunneling Undergr Space Technol 1987;2:319–33. http://dx.doi.org/10.1016/0886-7798(87)90043-5.

[21] Jansson A, Fernandez I, Berrocal CG, Rempling R. Experimental dataset for loads on hard rock shotcrete tunnel linings in a laboratory environment. Data Brief 2024;110920. http://dx.doi.org/10.1016/j.dib.2024.110920.

[22] Jansson A, Fernandez I, Berrocal CG, Rempling R. Investigation of the impact of concrete surface treatment methods on the interfacial bond strength. 43, Springer Science and Business Media B.V.; 2023, p. 925–34. http://dx.doi.org/10.1007/978-3-031-33211-1_83,

[23] Sjölander A, Hellgren R, Malm R, Ansell A. Verification of failure mechanisms and design philosophy for a bolt-anchored and fibre-reinforced shotcrete lining. Eng Fail Anal 2020;116. http://dx.doi.org/10.1016/j.engfailanal.2020.104741.